Nontrivial Periodic Coherent State in Globally Coupled Oscillators

Di Yuan*, Huijuan Geng, Jing Zhang, Shengnan Li, Junlong Tian†

Abstract—**In this work, we study the mean-field Kuramoto model with attractive (positive) and repulsive (negative) coupling strengths under an external pinning force. We consider the coupling strengths correlate with the natural frequencies of oscillators. It is found that the interplay between the correlations and the pinning force induces multistable coherent behaves like different forms of traveling wave states, stationary synchronous and novel non-stationary dynamical behave: a nontrivial periodic coherent state. The nontrivial periodic coherent state can be depicted by the phase distributions of oscillators, the phase distributions oscillate in a confined region periodically. Finally, the dynamical distribution regions of the system with the parameter scale are demonstrated.**

Index Terms—**Kuramoto model, external pinning force, attractive interaction, repulsive interaction, nontrivial periodic coherent state**

I. Introduction

Synchronization phenomenon exists widely in many subscience. They have been investigated according to phase models, which efficaciously describe systems of little coupled limit cycle oscillators. As a classic model, the Kuramoto model [1] has offered a pattern for studying synchronization in a broad scope of physical, biological and chemical domains, such as fireflies flashing in unison [2], electrochemical and spin-toque oscillators [3], laser networks [4-6], Josephson junction arrays [7], mercury beating-heart oscillators [8], electronic networks [9-11], population networks [12,13], and social networks [14-22].

The primordial Kuramoto model contains N phase oscillators, which are whole coupled together, and the equations take the following form:

$$\dot{\phi}_i = \omega_i + K\sum_{j=1}^{N}\Gamma_{ij}(\phi_j - \phi_i),\ \ \mathrm{i}=1,2,...,N, \tag{1}$$

where ϕ_i is the instantaneous phase for the i th oscillator, ω_i is the frequency for the i th oscillator, and Γ_{ij} is a 2π-period function accounting for the reciprocity between phase oscillators. The simple choice of $\Gamma_{ij}(\theta)=(1/N)\sin\theta$ leads to the classical Kuramoto model. K is the global interaction strength. The model's come down to hypothesis of sinusoidal interaction and infinite-range couplings allowed Kuramoto to achieve precise results for its quiescent states in the limit $N\to\infty$, an distinct phenomenon observed that the model's long-term behavior furcates from an incoherent behave to a fractionally coherent state at a critical interaction strength K_c. The coupling strength K was assumed is positive in the early time, corresponding to an attractive interaction between oscillators and the average field. The attractive coupling is apt to align the oscillators in phase. The negative is assigned for the coupling strength K later, the negative coupling as repulsive effect actuates oscillators separation and forms a phase distinction of π. When two different forms of couplings are added, the behaves of system becomes complicated. Hong and Strogatz considered positive and negative interactions in a mean field Kuramoto model [23, 24] and found a variety of dynamical behaviors including traveling wave states, partially synchronized states, and fully synchronized states. Borgers and Kopell studied the biological systems contain excitatory and inhibitory couplings [25]. Inhibitory interactions suppress the undesired synchronization and destabilize synchronized neural networks have been researched by Louzada *et al*. [26] and Freeman *et al*. [27], respectively. In human society, conformists positively follow the neighbors' opinion when they interact with neighbors. However, the contrarians refuse the neighbors' viewpoint all the time.

Compare with the earlier discussions of the Kuramoto model containing the positive and negative interactions. In the present work, we consider the Kuramoto model consist of attractive and repulsive coupling strengths under an external pinning force. Some researchers considered the pinning force in an active rotator [26–33]. Shinomoto and Kuramoto considered the phase change in active rotator models, they demonstrated two different scopes in the phase plot: a scope of time-periodic dynamical noticeable, and a scope of stable stationary synchronized behaves [34]. Hong studied a

Manuscript received June 29, 2021; revised October 13, 2021. This work is supported by the National Natural Science Foundation of China (Grant Nos. 11447001, 11475004), the Foundation for University Youth Key Teacher by the Henan Province (Grant No. 2019GGJS190), the Special Program for Basic Research of the Key Scientific Research Projects in Universities of Henan Province (Grant No. 21zx015), the Key Scientific and Technological Project of Henan Province (Grant No. 212102210484), the Scientific and Technological Project of Anyang City (Grant Nos. 2020028, 2021C01GX013, 2021C01SF020), and the Innovation Foundation for Students of Anyang Normal University (Grant Nos. X202010479097, 202110479091).

*Di Yuan is an associate Professor of School of Physics and Electrical Engineering, Anyang Normal University, Anyang, 455000, China (corresponding author, phone: 086-0372-3300041; e-mail: yuandi@aynu.edu.cn).

Huijuan Geng is a PhD of School of Physics and Electrical Engineering, Anyang Normal University, Anyang, 455000, China (e-mail: ghjhou@126.com).

Jing Zhang is an associate Professor of School of Physics and Electrical Engineering, Anyang Normal University, Anyang, 455000, China (e-mail: zj@aynu.edu.cn).

Shengnan Li is a student of School of Physics and Electrical Engineering, Anyang Normal University, Anyang, 455000, China (e-mail: 38617627@qq.com).

†Junlong Tian is a Professor of School of Physics and Electrical Engineering, Anyang Normal University, Anyang, 455000, China (corresponding author, phone: 086-0372-3300253; e-mail: tianjl@163.com).

coupled oscillator model, which contains the pinning force, and a peculiar dynamic state was found [35]. Through the investigation and study [36-42], we think that the Kuramoto model containing a pinning force could be better explored in some respects.

This work aims at analyzing the effects of pinning force to the dynamical behavior under the interactions between attractive and repulsive couplings. The paper is arranged as follows. We state the model and express some properties on the model in Sec. II. Sec. III presents the numerical results and shows the phase diagrams of the model with different types of relevance between the distributions of frequencies and the interaction strengths of oscillators. The work is summarized in Sec. IV.

II. Model

We give a thought to the network of N phase oscillators with a pinning force, and the phase of each oscillator is evolved by the following equations

$$\dot{\phi}_i = \omega_i + a\sin\phi_i + \frac{K_i}{N}\sum_{j=1}^{N}\sin(\phi_j - \phi_i), \quad i=1,2,...,N. \tag{2}$$

Where the frequency ω_i is selected stochastically from a Lorentzian probability distribution, $g(\omega)=\gamma/[\pi(\omega^2+\gamma^2)]$. Throughout this work, the width γ=0.05. The second part on the right-hand side of Eq. (2) is the pinning force, and the dynamics of excitable limit-cycle oscillators can be simulated by means of the pinning force [31, 32], and a on behalf of the intensity of pinning force. K_i reflects the response of the ith oscillator to the mean field. The oscillators in Eq. (2) can be divided into two sub-collections: the oscillators with positive coupling ($K_+ > 0$) are conformist, which affect attractively with the surplus oscillators, and the oscillators with negative coupling ($K_- < 0$) are contrarian, which repulse the others, respectively. N on behalf of the sum of phase oscillators in above system.

Next, we consider two cases for the interaction strengths correlate with the frequencies of oscillators. One case is that if $|\omega_i| < \omega_0$, the interaction strength of the ith oscillator is arranged as $K_i = K_+$ and $K_i = K_-$ for other oscillator, and the another case is that the second situation, if $|\omega_i| > \omega_0$, the interaction strength of the ith oscillator is arranged as $K_i = K_+$ and $K_i = K_-$ for other oscillator. The correlation distributions are as follows:

Case 1:

$$g(\omega,K)=\frac{\gamma}{(\omega^2+\gamma^2)\pi}[H(\omega_0-|\omega|)\delta(K-K_+)+(1-H(\omega_0-|\omega|))\delta(K-K_-)]$$

Case 2:

$$g(\omega,K)=\frac{\gamma}{(\omega^2+\gamma^2)\pi}[H(\omega_0-|\omega|)\delta(K-K_-)+(1-H(\omega_0-|\omega|))\delta(K-K_+)] \tag{3}$$

where H ($\cdot$) on behalf of Heaviside expression. The above two different relevant situations have respective significance. Let's hold the case 1 as an explanation, people in the mainstream share similar opinions in normal human society and they easy to get along with. On the contrary, there are radical who may be are apt to refuse the popular opinions. The case 1 may be a good choice for researcher to explore the dynamical behavior in such a present world.

Collective behavior of phase synchronization is generally portrayed by the complex order parameter, the complex characterization parameter $\mathrm{R}e^{i\Phi}$ which is expressed by

$$Z = \mathrm{R}e^{i\Phi} = \frac{1}{N}\sum_{j=1}^{N} e^{i\phi_j}, \tag{4}$$

where the Φ shows the average phase, and the real variant $0 \le \mathrm{R} \le 1$ shows the macroscopic order. Then, the Eq. (2) can be expressed according to R and Φ as

$$\dot{\phi}_i = \omega_i + a\sin\phi_i + K_i R\sin(\Phi - \phi_i), \quad i=1,2,...,N, \tag{5}$$

which shows the development of the ith oscillator autonomously according to R and Φ. We explore collective synchronization of the system, each subpopulation's synchronization also an important observed quantity. The synchronization behaviors of the conformists and contrarians are expressed by $Z_\pm = \mathrm{R}_\pm e^{i\Phi_\pm} = (1/N_\pm)\sum_{j\in S_\pm} e^{i\phi_j}$, where $S_\pm$ denote the ensembles of conformists and contrarians, respectively, and $N_\pm$ denote the total quantities of positive and negative of oscillators, respectively.

III. Results and Discussion

To explore the dynamical behaviors given by the Eq. (2), we performed numerical simulations by Runge–Kutta procedure of fourth-order, we assign the time interval δt = 0.01. From start to finish, we measured the quantities of interest by averaging and discarding the transient process. In addition, we set $K_- = -1.5$, $K_+ = 4.0$, $a = 0.01$, $N = 10000$ and $\gamma = 0.05$ unless specified.

A. Situation with $K_i = K_-$ for $|\omega_i| > \omega_0$ and $K_i = K_+$ otherwise

At present, we consider the situation with $K_i = K_-$ for $|\omega_i| > \omega_0$ and $K_i = K_+$ for other oscillator. We first investigated the synchronization plots of the order parameters R, R_- and R_+ opposite ω_0. Fig. 1(a) shows the amplitudes against ω_0. When $\omega_0 = 0$, the system has only contranrians. When the cut-off frequency ω_0 increases gradually, the number of conformists also increases, we can see that the system presents several different regimes from Fig. 1(a), which mean different dynamical states in this system. It is shown that the amplitude of R_+ almost stays around 1, which indicates the conformists keep high synchronization for very low ω_0. However, the amplitudes of R and R_- manifest a doughty dependence on ω_0. So, we can distinguish the several different regimes of ω_0 according to the change of amplitudes of R and R_-, the break points are $\omega_{0,1}$ =0.015, $\omega_{0,2}$ = 0.021, $\omega_{0,3}$ = 0.064 and $\omega_{0,4}$ = 0.088, respectively.

We characterize these different dynamics by some quantities of observation, such as the speed of a traveling wave Ω and the phase difference $\Delta\Phi$. The quantity of observation Ω is defined as $\Omega = (1/N)\times\sum_{j=1}^{N}\langle\dot{\phi}_j\rangle$, when $\Omega \neq 0$, the system presents a mobile dynamic state behavior. The observed quantity of $\Delta\Phi$ ($\Delta\Phi = \Phi_+ - \Phi_-$) denotes the phase

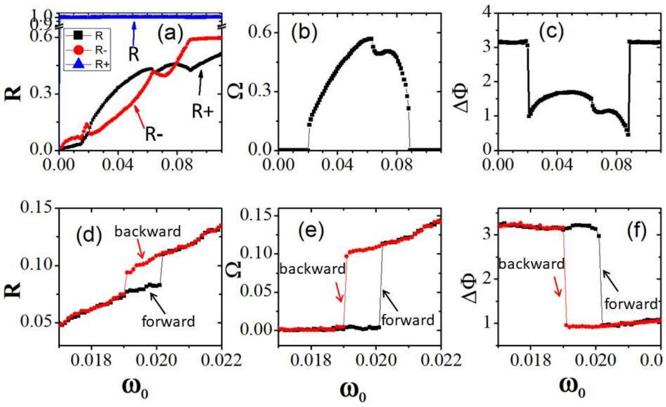

Fig. 1 (color online) Real parts (a) of the order parameter R (in black square), R_- (in red circle), and R_+ (in blue triangle) against ω_0. (b) Traveling speed Ω of wave opposite ω_0. (c) $\Delta\Phi$ between the mean phases of the different order parameters of conformists Z_+ and contrarians Z_- opposite ω_0. (d)–(f) The parameter scope in (a)–(c) is enlarged. In above three graphs, forward continuation (with black) and backward continuation (with red) transition diagrams are presented. $K_- = -1.5$, $K_+ = 4.0$, $a = 0.01$, and $\gamma = 0.05$.

difference between the average phases of positive and negative of oscillators. In Fig. 1(b), we plot the Ω against ω_0, it is shown that the quantity Ω becomes nonzero in the region of $\omega_0 \in (\omega_{0,2}, \omega_{0,4})$. Fig. 1(c) presents the $\Delta\Phi$ against ω_0 in the same region, it is shown that $\Delta\Phi$ diverges from π. By comparing Figs. 1(b) and Figs. 1(c), we know that the mobile state exists in the region of $\omega_0 \in (\omega_{0,2}, \omega_{0,4})$. In addition, it is noteworthy that the transition diagrams of R (Fig. 1(a)), Ω (Fig. 1(b)) and $\Delta\Phi$ (Fig. 1(c)) are not smooth continuous in the region of $\omega_0 \in (\omega_{0,2}, \omega_{0,4})$, there is a jump at around $\omega_{0,3}$, which implies that mobile dynamic states are divided into two parts, each part corresponding to one type state. We can see clearly that the π state emerges in the regions of $\omega_0 < \omega_{0,1}$ or $\omega_0 > \omega_{0,4}$ in Figs. 1(b) and (c). The π state corresponding to the conformists and contrarians gather into one synchronized cluster, respectively. The two peaks of the phase distributions have a separation of an angle of π.

From Fig. 1 (a), we can see that the transition at around $\omega_{0,2}$ is a discontinuous one. Figs. 1(d), 1(e) and 1(f) show the transition diagrams for the forward and backward transition. The forward transition diagram was calculated by adding continuously the value of ω_0, these quantities R, Ω and $\Delta\Phi$ were computed for $\omega_0, \omega_0 + \delta\omega_0, \ldots, \omega_0 + n\delta\omega_0$, that is to say, the tag end state of the prior one ω_0 is the initial conditions for next one. On the contrary, the backward transition plot is calculated by shrinking continuously the value of ω_0. Figs. 1(d), 1(e) and 1(f) show that the strong hysteresis exists at around $\omega_{0,2}$, and the emergence of hysteresis manifests the coexistence of the cluster coherent states and the traveling dynamic behaviors in this region.

We now use effective frequency to characterize the dynamics in different regimes. The effective frequency of corresponding oscillator is expressed as $\omega_e = \langle d\phi/dt \rangle_t$. The effective frequency ω_e is computed for every oscillator as shown in Figs. 2(a), 2(b), 2(c) and 2(d) with different ω_0, respectively. Correspondingly, the instantaneous plots of the phases are shown in Figs. 2(e), 2(f), 2(g) and 2(h), and all oscillators have been sorted on the basis of their natural frequencies. For example, if $\omega_i < \omega_j$, then $n_i < n_j$. We know that π state is presented in the scope of $\omega_0 < \omega_{0,1}$. Figs. 2(a) shows the frequency $\omega_e(\omega)$ with the oscillators' frequencies for $\omega_0 = 0.01$, it is easy to see that the graph has one plateau $\omega_e = 0$, the plateau implies that there are some oscillators phase-locked to the mean field. Correspondingly, it is shown that a small part of oscillators are synchronized from the snapshot of phases shown in Fig. 2(e). In addition, it should be noted that the plateau is consecutive and symmetric about $\omega = 0$.

For $\omega_{0,2} < \omega_0 < \omega_{0,3}$, as shown in Figs. 2(b) and 2(f) for $\omega_0 = 0.04$, the plot of $\omega_e(\omega)$ turns into skew symmetric about $\omega = 0$, the platform is inconsecutive and splits into two discrete parts, the instantaneous plot of phases shows that one plateau for conformists and the other platform for part of the negative of oscillators. The Fig. 2(b) shows that the effective frequency on the platform deviates from $\omega_e = 0$. We know that the average field vibrates at a frequency distinguish from the population's effective frequency for a mobile wave state [21]. Therefore, the plateau deviates from $\omega_e = 0$ in Fig. 2(b) implies the existence of traveling wave states. For $\omega_{0,3} < \omega_0 < \omega_{0,4}$, as shown in Figs. 2(c) and 2(g), the plot of $\omega_e(\omega)$ continues to be skew symmetric about $\omega = 0$ for $\omega_0 = 0.08$, it is noteworthy that the platform is recovered to be a consecutive one in the plot $\omega_e(\omega)$. By comparing Fig. 2(b) and Fig.2 (c), we can distinguish the every types of mobile dynamic states on different positions of $\omega_{0,3}$. For $\omega_0 > \omega_{0,4}$, we take $\omega_0 = 0.1$ as an example, as shown in Figs. 2(d) and 2(h). From Fig. 2(d), we can see that the plateau is return to a symmetric one about $\omega = 0$,

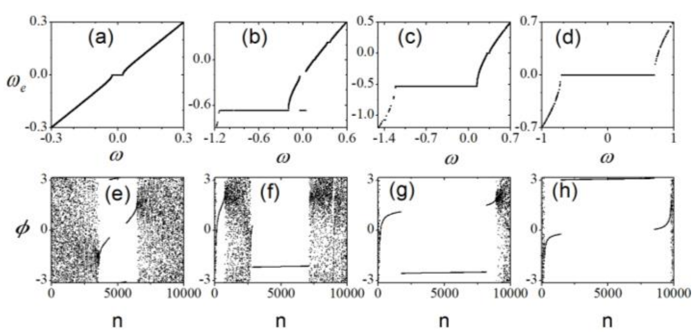

Fig. 2 (color online) Effective frequencies ω_e are shown as a function of ω_i in above (a), (b), (c) and (d). instantaneous plots of the oscillators are presented in above (e), (f), (g) and (h). (a, e) $\omega_0 = 0.01$; (b, f) $\omega_0 = 0.04$; (c, g) $\omega_0 = 0.08$; (d, h) $\omega_0 = 0.1$; $K_- = -1.5$, $K_+ = 4.0$, $a = 0.01$ and $\gamma = 0.05$.

correspondingly, the π states are recovered in the system.

Through the above analysis, we have identified several different dynamical states in the model Eq. (2). In addition, it is exciting that this system still presents a novel nonstationary dynamical behavior in the scope of $\omega_0 \in (\omega_{0,1},\ \omega_{0,2})$. The novel state is characterized by the phase distributions with evolutions of as shown in Fig. 3(a) (the conformists) and Fig. 3(b) (the contrarians) for $\omega_0 = 0.018$. We can see a fire-new dynamical state from Figs. 3(a) and 3(b), which is different from the mobile wave state and the π state found by Hong and Strogatz [21]. First, the phase distributions are nonstationary, second, the distributions of phase do not mobile along the phase space, third, the phase distributions oscillate in a limited scope periodically. In addition, the phase distribution of contrarians is bimodal, and the reason is that there is a fraction of contrarians which get synchronized, and the contrarians with positive frequencies are fixed to a diverse phase in contrasting to some oscillators with negative frequencies. Furthermore, we investigated the nontrivial periodic coherent state from the evolution of oscillators for phase. As exhibited in Fig. 3(c), it is obvious that there exist several clusters, and the phase change time dependent periodically of each oscillator. In addition, the period of evolutions for the phase distributions is identical to that for phase of oscillators by contrasting Figs. 3(a), 3(b) and 3(c).

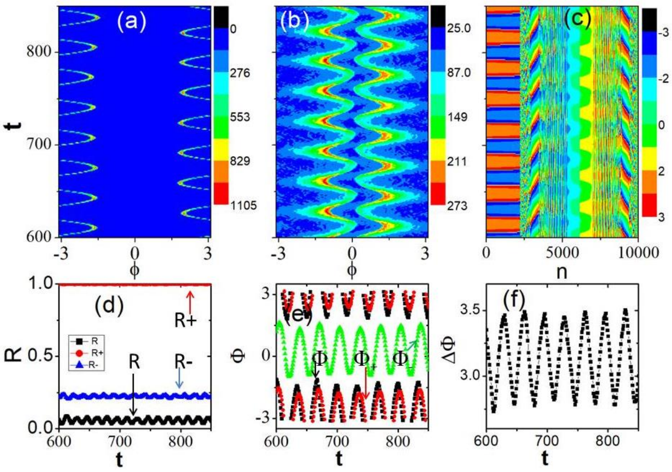

Fig. 3 (color online) Time variations of the phase distributions for the conformists (a) and contrarians (b), respectively. (c) Time evolutions of oscillators' phases. Colors in (a)-(c) on behalf of the number of oscillators; specific value can be confirmed according to color bars. (d) Amplitudes R (black), R_- (blue), and R_+ (red), of the order parameter. (e) average phase Φ (black), Φ_- (bright green), and Φ_+ (red). (f) phase difference $\Delta\Phi$. $\Delta\Phi$ oscillates periodically. $\omega_0 = 0.018$, $K_- = -1.5, K_+ = 4.0, a = 0.01$ and $\gamma = 0.05$.

The nontrivial periodic coherent state also can be validated through the amplitudes, R and $R_\pm$, of the order parameter. In Fig. 3(d), we plot the evolutions of amplitudes, R (black), R_- (red) and R_+ (blue), of the order parameters. Fig. 3(e) manifests the Time variations of average phases Φ (the curve one with black), Φ_+ (the curve one with red) and Φ_- (the curve one with bright green). It is shown that the amplitudes and the average phases oscillate periodically with time. In Fig. 3(f), we present the evolution of the phase difference $\Delta\Phi$ between conformists and contrarians, it is shown that the $\Delta\Phi$ also oscillates periodically.

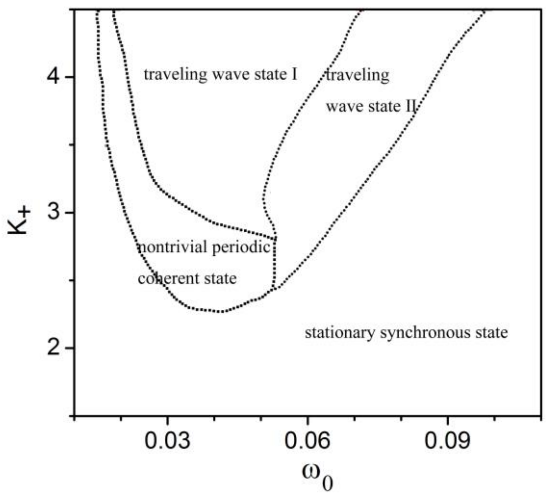

Fig. 4 (color online) Bifurcation plot of the system (2) on the space of K_+ and ω_0. The different dynamics are divided by the different curves. Nontrivial periodic coherent states locate at the lower ω_0 border of the traveling dynamic state. Traveling dynamic states are apt to appear at large K_+. Traveling wave state I is the traveling wave state in which the platform in plot of $\omega_e(\omega)$ is split into two parts. Traveling wave state II is the traveling wave state in which the platform in plot of $\omega_e(\omega)$ is concatenated. The stationary synchronous state can be found below the nontrivial periodic coherent state and the traveling wave state. $K_- = -1.5, a = 0.01$ and $\gamma = 0.05$. Here $K_i = K_+$ for $|\omega_i| < \omega_0$ and $K_i = K_-$ for other oscillators.

The dynamics in the system (2) for the present relevance between the interaction strengths and the distributions of frequencies is summarized as shown in Fig. 4, we plot the bifurcation diagram as functions of K_+ and ω_0. From Fig. 4, we can distinguish the region for the different dynamical states. We find that the nontrivial periodic coherent states locate at the lower ω_0 boundary of the traveling wave state. The traveling dynamic states are apt to appear at large K_+ and the traveling dynamic state appears in a broader window with the increase of ω_0. Below the nontrivial periodic coherent behavior and the traveling dynamic state, we can find the stationary synchronous state. It is worth noting that different dynamics in the model (2) can be realized by changing the coupling strength ω_0 at the intermediate K_+, which reflects the important role of cut-off frequency ω_0 in this system.

B. Situation with $K_i = K_+$ for $|\omega_i| > \omega_0$ and $K_i = K_-$ otherwise

We now consider the situation with $K_i = K_+$ for $|\omega_i| > \omega_0$ and $K_i = K_-$ for other oscillators. In this situation, when the cut-off frequency ω_0 increases gradually, correspondingly, the number of contrarians increases. In Fig. 5(a), we draw the

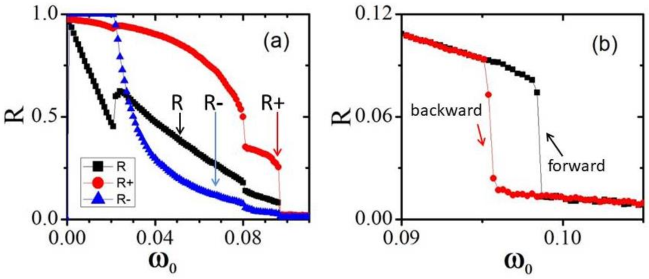

Fig. 5 (color online) (a) Real parts of the cpmplex parameters R (black), R_- (blue), and R_+ (red) opposite ω_0. (b) Amplitude R with a narrow range of ω_0. In this map, forward (black) continuation and backward (red) continuation are manifested. $K_- = -1.5$, $K_+ = 4.0$, $a = 0.01$ and $\gamma = 0.05$. Here $K_i = K_+$ for $|\omega_i| > \omega_0$ and $K_i = K_-$ for other oscillators.

the amplitudes of the order parameters R and $R_\pm$ against ω_0, it is shown that there are several different dynamics in this system. With the increase of ω_0, this system successively presents rich dynamics, such as stationary synchronous state, the traveling wave state I (the platform in the map of $\omega_e(\omega)$ is split into two pieces), the traveling waves state II (the platform in the map of $\omega_e(\omega)$ is a concatenated one), and the disorder state. In addition, we find that the transition between the traveling wave state II and the disorder state has a jump. We use the forward and the backward continuation diagram to investigate the discontinuous change as manifested in Fig. 5(b), the hysteresis is displayed. Correspondingly, we can know that the traveling wave state II and the incoherent state can coexist in this region.

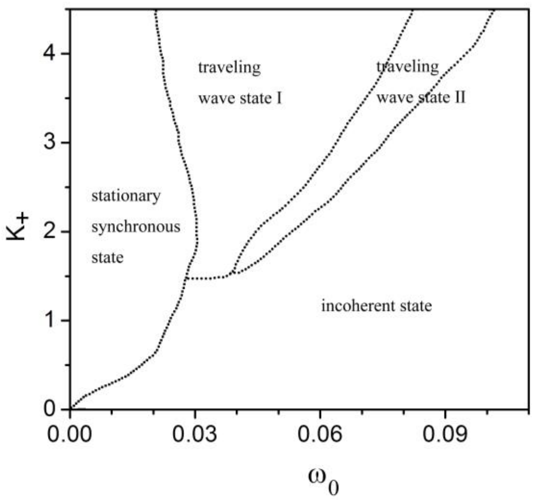

Fig. 6 (color online) Bifurcation map of the system model (2) on the scope of K_+ and ω_0. Different dynamics are divided by the different curves. Stationary synchronous state situates at the lower ω_0 border of the incoherent state and traveling wave state. Traveling wave state is apt to appear at large K_+ and at middle ω_0. On the right sides of the stationary synchronous behavior and the traveling dynamic state are the incoherent state. $K_- = -1.5$, $a = 0.01$ and $\gamma = 0.05$. Here $K_i = K_+$ for $|\omega_i| > \omega_0$ and $K_i = K_-$ for other oscillators.

In Fig. 6, we present the bifurcation diagram on the space of K_+ and ω_0 on the dynamics of the model (2) with the current correlation. It is obvious that different dynamical regions can be distinguished from Fig. 6. On the right sides of the stationary synchronous dynamic state and the traveling wave state are the incoherent state. The stationary synchronous state can be found situate at the lower ω_0 border of the incoherent states, and the traveling wave state is apt to appear at large K_+ and at middle value of ω_0.

IV. CONCLUSIONS

In this research work, the Kuramoto model of whole coupled oscillators with an extrinsic pinning force is investigated, in which conformists with positive interaction strength and contrarians with negative interaction strength. In this system, two diverse relevance of the coupling strengths correlate with the natural frequencies of oscillators are considered, rich synchronous dynamical behaviors are found. We find a novel nonstationary dynamic state, the phase distributions of oscillators can be used to characterize the periodic coherent state. Because of the effects of pinning force to the model (2), we find that the phase distribution of contrarians is bimodal, the phase distributions and the phase difference oscillate in a confined region periodically. The traveling wave state presented in this system can be ascribed to two species. The diverse types of traveling wave dynamic state can be distinguished by the graph $\omega_e(\omega)$ of effective frequency. In addition, we manifest the bifurcation diagrams of the system model (2) for different cases from which the parameter scope of the nontrivial periodic coherent state, the stationary synchronous state and the traveling wave dynamic state can be obtained.

REFERENCES

[1] Kuramoto Y. "In international symposium on mathematical problems in theoretical physics," In: Araki H, editor. Lecture Notes in Physics. New York: Springer, vol. 39, pp. 420-422, 1975.
[2] Buck J., and Buck E. "Synchronous fireflies," Sci. Am., vol. 234, pp. 74-85,1976.
[3] Kiss I. Z. et al. "Emerging coherence in a population of chemical oscillators," Science, vol. 296, pp. 1676-1678, 2002.
[4] Larger L., Penkovsky B., and Maistrenko Y. "Laser chimeras as a paradigm for multistable patterns in complex systems," Nat. Commun., vol. 6, pp. 7752, 2015.
[5] Böhm F., Zakharova A., Schöll E., and Lüdge K. "Amplitude-phase coupling drives chimera states in globally coupled laser networks," Phys. Rev. E, vol. 91, pp. 040901, 2015.
[6] Javaloyes J., Perrin M., and Politi A. "Collective atomic recoil laser as a synchronization transition," Phys. Rev. E, vol. 78, pp. 011108, 2008.
[7] Wiesenfeld K., Colet P., and Strogatz S. H. "Synchronization transitions in a disordered Josephson series array," Phys. Rev. Lett., vol. 76, pp. 404, 1996.
[8] Kumar P., Verma D. K., Parmananda P., and Boccaletti S. "Chimera states: coexistence of coherence and incoherence in networks of coupled oscillators," Phys. Rev. E, vol. 91, pp. 062909, 2015.
[9] Heide D., Schäfer M., and Greiner M. "Robustness of networks against fluctuation-induced cascading failures," Phys. Rev. E, vol. 77, pp. 056103, 2008.
[10] Simonsen I. et al. "Transient dynamics increasing network vulnerability to cascading failures," Phys. Rev. Lett., vol. 100, pp. 218701, 2008.
[11] Dörfler F., Chertkov M., and Bullo F. "Synchronization in complex oscillator networks and smart grids," Proc. Natl Acad. Sci., vol. 110, pp. 2005-2010, 2013.
[12] A. Zakharova, M. Kapeller, and E. Schöll. "Chimera Death: Symmetry Breaking in Dynamical Networks," Phys. Rev. Lett., vol. 112, pp. 154101, 2014.

[13] Néda Z. et al. "Physics of the rhythmic applause," Phys. Rev. E, vol. 61, pp. 6987-6992, 2000.
[14] Gambuzza L. V. et al. "Experimental investigation of chimera states with quiescent and synchronous domains in coupled electronic oscillators," Phys. Rev. E, vol. 90, pp. 032905, 2014.
[15] Hizanidis J., Lazarides N., and Tsironis G. P. "Chimeras in locally coupled squids: Robust chimera states in SQUID metamaterials with local interactions," Phys. Rev. E, vol. 94, pp. 032219, 2016.
[16] Makarov V. V. et al. "Alterations in Salience Network Functional connectivity in Individuals with Restless Legs Syndrome," Sci. Rep., vol. 7, pp. 17246, 2017.
[17] Daniel J. Korchinski et al. "Criticality in Spreading Processes without timescale Separation and the Critical Brain Hypothesis," Phys. Rev. X, vol. 11, pp. 021059, 2021.
[18] Hendrik S. Sylvain F. and Laura H., "When network bridges foster consensus bounded confidence models in networked societies," Phys. Rev. Research, vol. 3, pp. 023208, 2021.
[19] Andrea N. Alessandro P. Marco R., and Domenico G, "Analytical and cellular automaton approach to a generalized SEIR model for infection spread in an open crowded space," Phys. Rev. Research, vol. 2, pp. 043379, 2020.
[20] Simon M. Asher A. F., and Nir D., "Experimental demonstration of crowd synchrony and first-order transition with lasers, Phys. Rev. Research," vol. 2, pp. 043220, 2020.
[21] E. Ramirez-Juidias, A. Madueno-Luna, and J.M. Madueno-Luna, "A New Mathematical Model of Slope Stability Analysis," Engineering Letters, vol. 29, no. 3, pp. 913-918, 2021.
[22] Yanhong Yao, and Hejun Yao, "Finite-time Control of Complex Networked Systems with Structural Uncertainty and Network Induced Delay," IAENG International Journal of Applied Mathematics, vol. 51, no. 3, pp. 508-514, 2021.
[23] Hong, H., and Strogatz, S. "Kuramoto model of coupled oscillators with positive and negative coupling parameters: An example of conformist and contrarian oscillators," Phys. Rev. Lett., vol. 106, pp. 054102, 2011.
[24] Hong, H., and Strogatz, S. "Conformists and contrarians in a kuramoto model with identical natural frequencies," Phys. Rev. E, vol. 84, pp. 046202, 2011.
[25] Borgers C., and Kopell N. "Synchronization in networks of excitatory and inhibitory neurons with sparse, random connectivity," Neural Comput., vol. 15, pp. 509-538, 2003.
[26] Louzada V. H. P. et al. "How to suppress undesired synchronization," Sci. Rep., vol. 2, pp. 00658, 2012.
[27] Freeman G. M. et al. "GABA networks destabilize genetic oscillations in the circadian pacemaker," Neuron, vol. 78, pp. 799-806, 2013.
[28] Sakaguchi H. "Cooperative phenomena in coupled oscillator systems under external fields," Prog. Theor. Phys., vol. 79, no. 1, pp. 39-48, 1988.
[29] Kori H. and Mikhailov A. S. "Strong effects of network architecture in the entrainment of coupled oscillator systems," Phys. Rev. E, vol. 74, pp. 066115, 2006.
[30] Antonsen T. M., Faghih R. T., Girvan M., Ott E., and Platig J. "Low dimensional behavior of large systems of globally coupled oscillators," Chaos vol. 18, no. 3, pp. 037112, 2008.
[31] Park S. H. and Kim S. "Noise-induced phase transitions in globally coupled active rotators," Phys. Rev. E, vol. 53, pp. 4, 1996.
[32] Sunny Orike, and Joseph Diema Enoch, "A Smart Microcomputer-Based Controlled Device for Electrically Powered Gadgets," Lecture Notes in Engineering and Computer Science: Proceedings of the World Congress on Engineering and Computer Science, October, pp. 22-24, 2019.
[33] Eduardo Giraldo, "Real-time Control of a Magnetic Levitation System for Time-varying Reference Tracking," IAENG International Journal of Applied Mathematics, vol. 51, no. 3, pp. 792-798, 2021.
[34] Shinomoto S. and Kuramoto Y. "Phase transitions in active rotator systems," Prog. Theor. Phys., vol. 75, no. 5, pp. 1105-1110, 1986.
[35] Hong H. "Periodic synchronization and chimera in conformist and contrarian oscillators," Phys. Rev. E, vol. 89, no. 6, pp. 062924, 2014.
[36] Di Yuan *et al*. "Multistable states in a system of coupled phase oscillators with inertia," Scientific Reports, vol. 7, pp. 42178, 2017.
[37] Di Yuan *et al*. "Periodic synchronization in a system of coupled phase oscillators with attractive and repulsive interactions," Frontiers of Physics, vol. 13, no. 3, pp. 130504, 2018.
[38] Felix G. Eckehard O., and Sven B. "Dynamics of opinion expression," Phys. Rev. E, vol. 102, pp. 042303, 2020.
[39] Rico B. Serhiy Y., and Eckehard S. "What adaptive neuronal networks teach us about power grids," Phys. Rev. E, vol. 103, pp. 042315, 2021.
[40] Guo-Xiu Jing, Dong-Sheng Shuai, and Bing Zhang, "Research on Control Strategy of AC DC Hybrid Power Distribution Network with Multiple Voltage Levels," Engineering Letters, vol. 29, no. 3, pp. 881-886, 2021.
[41] Iromi R Paranavithana, and Viraj R Kalansuriya, "Deep Convolutional Neural Network Model for Tea Bud(s) Classification," IAENG International Journal of Computer Science, vol. 48, no. 3, pp. 599-604, 2021.
[42] Muhammad Irfan, Faizir Ramlie, Widianto, Merinda Lestandy, and Amrul Faruq, "Prediction of Residential Building Energy Efficiency Performance using Deep Neural Network," IAENG International Journal of Computer Science, vol. 48, no. 3, pp. 731-737, 2021.